Molecular Dynamics Study of Anisotropic Lattice Diffusion in Cr_2O_3

P. Cao, D. M. Wells, M. P. Short

March 28, 2016

Abstract

Charge-corrected molecular dynamics (MD) studies of anion and cation self-diffusion, as well as cation dopant diffusion, have been performed using nudged elastic band (NEB) analysis on $\alpha - Cr_2O_3$. Non-negligible anisotropy in the diffusion coefficients between a- and c-axes, increasing in magnitude with decreasing temperature, was observed for all species studied (Cr^{3+}, O^{2-}, Fe^{3+}, Ni^{2+}). Trends in relative diffusivities, as well as absolute orders of magnitude, agree well with multiple experimental measurements. Because of the ubiquitous technological importance of Cr_2O_3 as the most frequently used corrosion-protecting passivation layer, especially on stainless steel, any method of reducing transport through Cr_2O_3 has profound implications for the reduction and control of corrosion.

1 Introduction

Chromium oxide ($\alpha - Cr_2O_3$) is arguably the world's most important oxide. It functions as the primary passivating protective layer of the world's most utilized corrosion-resistant structural material, stainless steel. Currently the production of Cr_2O_3-passivated stainless steels continues to grow expotentially, reaching 41.7 million metric tons in 2014 [1], underpinning critical infrastructures ranging from bridges, to buildings, to nuclear reactors. The continued corrosion-based upkeep cost of stainless steel alone reaching $\$___$billion pear year worldwide [REF - get from Ballinger]. Therefore, any deterministic ways of slowing the progress of oxygen penetration from the environment into the metal, or conversely of metal escape from the metal into the environment, however small, would constitute a substantial reduction in the total costs of corrosion worldwide. Even a 10% reduction in corrosion rate could save $\$___$billion per year, in addition to increasing inspection intervals and decreasing failure rates of Cr_2O_3-passivated components.

One well-known method of controlling corrosion rates governed by ionic transport is to control the texture or anisotropy of the material. This has been well-characterized in stainless steels, where the corrosion rates of both 304 [2] and 316 [3] were found to directly vary with local crystallographic orientation, separately from the effects of stress-induced α'-martensite. While the substrate orientation was cited as the determining factor, it is almost certainly the character of the passive Cr_2O_3 layer which controls the corrosion rate. The character of the oxide layer, including its orientation, is itself almost certainly determined by the orientation of the underlying substrate. These studies point to the texture of the underlying steel changing the character of the oxide layer on top. This effect has been observed in other passivating materials as well. Kudelka et al showed how differently oriented grains of Ti corrode at different rates, by studying oxide texture and thicknesses on individual grains in the same experiment [4]. In addition, Hoseini et al showed varying rates of corrosion by impedance spectroscopy to vary with grain orientation in annealed and severly plasticly deformed (SPD) titanium, attributing the change in corrosion rate specifically to substrate grain orientation [5]. Even oxidation of pure platinum exhibits a clear dependence on the underlying metal orientation [6]. Clearly the effect of underlying metal orientation changes the nature of the passivating, corrosion-resistant oxide layer on top.

For passivating materials which function as effective diffusion barriers [7], the difference between directionally-different diffusivities will determine the relative, texture-dependent corrosion rates through these materials. Examples of anisotropic cation and anion diffusion through non-cubic oxides exist throughout the literature. These will be reivewed briefly here, with emphasis on those that explore the diffusion mechanisms, not just

the rates, behind cation and anion transport. Chroneos et al showed preferential oxygen diffusion in the *a*-*b* plane of tetragonal $La_2NiO_{4+\delta}$ using MD simulations which explained formerly anomalous experimental measurements which varied by a factor of up to 4.5 [8]. Kendrick et al showed the importance of mechanistic understanding in predicting the diffusivity of oxygen through Ga-based oxides, with their results agreeing well with experiments [9]. The critical importance of understanding diffusion mechanisms through anisotropic oxides in the form of solid oxide fuel cells was recently highlighted by Chroneos et al [10], underscoring the need for more than the standard experiments/simulations showing simply gross rates of transport without explanation.

Dopants can also change oxygen penetration through oxides, either by substition or by ordering. Parfitt et al showed that cation disorder changes oxygen anion diffusion anisotropy [11], showing how cation ordering can affect anion transport through oxides. [MORE TO COME ON DOPING SOON]

Transport of cations and anions specifically through Cr_2O_3 has been experimentally and theoretically studied, though to a degree far lower than would be expected given its technological importance. The experimental literature is more extensive, as tracer experiments of oxygen and cation transport have been quantified by multiple groups. Hagel experimentally found that anion diffusion is slower through Cr_2O_3 compared to cation diffusion [12]. Sabioni et al. studied the diffusion of oxygen [13], manganese [14], chromium [15], and iron [16] through chromia polycrystals and thin films by secondary ion mass spectroscopy (SIMS), eventually finding that oxygen diffusivity is faster than that of chromium in Cr_2O_3. Lobnig et al also used tracer experiments to study the diffusion of Cr, Fe, and Ni through Cr_2O_3 [17] as functions of time, while Tsai et al [18] and Hoshino et al [19] experimentally studied the mechanisms of diffusion of Cr and O through Cr_2O_3. In particular, Hoshino et al specifically studied *a*- vs. *c*-axis oxygen anion diffusion, and found *c*-axis diffusion to be faster [19]. The literature concerning simulations of ionic transport *through* Cr_2O_3 are surprisingly scarce, though studies of surface structure are more common. Catlow et al [20] and Vaari [21] have predicted diffusion coefficients of cations and anions through Cr_2O_3 with comparisons to experimental values, showing mixed results. Because $\alpha - Cr_2O_3$ has a hexagonal close-packed (HCP) crystal structure with a c/a axis ratio of 2.74 over a very wide pressure range [22], any application utilizing $\alpha - Cr_2O_3$ as a passivation layer, from near-vacuum to ultra-high pressure, should benefit from the same texture-based gains in transport resistance. Therefore, precise knowledge of the orientation-dependent transport rates determines whether this strategy can succeed.

In this manuscript, we present detailed, mechanism-based molecular dynamics simulations of oxygen and cation (Fe, Ni, Cr) diffusion through $\alpha - Cr_2O_3$. A combination of defect formation energies, nudged elastic band (NEB) analysis, and extrapolation to lower temperatures via defect population scaling is shown to yield diffusion coefficients similar to those in the experimental results above. Most interesting is a clear anisotropy observed for both oxygen and cations, which increases at lower temperatures, pointing to the potentially enhanced corrosion resistance of $\alpha - Cr_2O_3$ at ___ orientations.

2 Methods

The LAMMPS MD code [23] was used in all simulations in this study. The diffusion coefficients of Fe^{3+}, Cr^{3+}, Ni^{3+}, and O^{2-} were all studied in $\alpha - Cr_2O_3$ directly at temperatures ranging from 1200-2000K. The effect of Fe^{3+} and Ni^{2+} cation dopant concentrations on the diffusion rate of O^{2-} up to concentrations of 0.15 atom fraction was also quantified.

The interactions between self-ions, dopant ions, and combinations thereof in $\alpha - Cr_2O_3$ were modeled by combining a short range Buckingham potential and a longer range Coulombic potential. The Buckingham potential is specifically chosen for its ability to model short-range charged defect interactions [REFs], as well as maintaining overall charge neurality of the MD simulation. The Coulombic potential models charge attraction/repulsion effects between ions, at distances greater than the atomic radii. The potential for the interaction between two ions i and j at a distance r is defined by Equation 1:

$$U_{ij}(r) = A_{ij}e^{-r/\rho_{ij}} - \frac{C_{ij}}{r_{ij}} + \frac{q_i q_j}{4\pi\epsilon_0 r_{ij}} \tag{1}$$

where the parameters A, ρ, and C are taken from the previous studies of Grimes et al and [24, 25]. Table 1 lists the parameters and references used for the various ions in this study. ___ et al had already performed validation

Ion Pair	$A_{ij}\,(eV)$	$\rho_{ij}\,(\text{Å})$	$C_{ij}\left(\frac{eV}{\text{Å}^6}\right)$	Ref.
$O^{2-} - O^{2-}$	9547.96	0.2192	32.0	[24]
$O^{2-} - Fe^{3+}$				
$O^{2-} - Cr^{3+}$	1204.18	0.3165	0.0	[24]
$O^{2-} - Ni^{3+}$				
$Fe^{3+} - Fe^{3+}$				
$Fe^{3+} - Cr^{3+}$				
$Fe^{3+} - Ni^{3+}$				
$Cr^{3+} - Fe^{3+}$				
$Cr^{3+} - Ni^{3+}$				
$Ni^{3+} - Ni^{3+}$				

Table 1: Parameters used in the mixed Buckingham-Coulomb potential for ion pairs in this study

Figure 1: Schematic of unit cell used in the simulations in this study

of these potentials, by studying ___ [PENGHUI, PLEASE FILL IN JUSTIFICATION FOR POTENTIAL USAGE HERE]

Like $\alpha - Al_2O_3$ and Fe_2O_3 , $\alpha - Cr_2O_3$ has the corundum structure. [ADD UNIT CELL DESCRIPTION]. Simulations were carried out using a 18×18×18 hexagonal supercell containing 58,320 atoms as shown in Figure 1. Periodic boundary conditions were used in all three directions. To study vacancy- and interstitial-assisted ion diffusion, ions were randomly inserted or deleted in the system. In these simulations, vacancy and interstital defects were studied at concentrations of 0.0008 at different temperatures, with low-temperature extrapolation performed by adjusting diffusion coefficients (D) for lower numbers of thermally stable vacancies following Equation 2:

$$D\left(T\right) = \alpha a^2 C\left(T\right)\omega = \alpha a^2 C\left(T\right) f_{Debye} e^{-E_m/k_B T} \tag{2}$$

where ω is the successful jump frequency of an ion from one site to another, f_{Debye} is the jump attempt frequency, E_m is the defect migration energy, k_B is Boltzmann's constant, T is the system temperature, α is a crystallographic constant relating the jump distance to the lattice parameter, a is the lattice parameter, and $C\left(T\right)$ is the thermally stable population of a particular defect. $C\left(T\right)$ can be defined by Equation 3:

$$C = e^{-E_f/k_B T} \tag{3}$$

where E_f is the defect formation energy. The above diffusivity equation can therefore be written by Equation :

$$D\left(T\right) = \alpha a^2 f_{Debye} e^{-\left(E_f + E_m\right)/k_B T} \tag{4}$$

Before the diffusion coefficient calculation, the system is relaxted at zero pressure for 100 ps in the NPT (constant number of atoms, pressure and temperature) and another 100 ps run is performed in the NVT ensemble (constant number of atoms, volume and temperature). The Nose-Hoover thermostat is used in time intergration and the time step is set to be 1 fs. The ion diffusion was determinated measureing mean square displacement (MSD) of ions as a function of time at a range of temperatures. The MSD of ion is described by Equation 5:

$$\left\langle \Delta r^2\left(t\right)\right\rangle = \frac{1}{N}\sum_{i=1}^{n}\left[r_i\left(t + t_0\right) - r_i\left(t_0\right)\right]^2 \tag{5}$$

where N is total number of the ion in the system, r(t 0) is initial reference position at time t 0 and r(t) is position at time t + t 0 . The diffusivity that relates MSD to the observe time t is defined in Equation 6:

$$D = \frac{\left\langle r^2\left(t\right)\right\rangle}{2d \times t} \tag{6}$$

where d is dimensionality of the system. Then, the diffusivities of ions along the c-axis, in the ab-plane and in three dimensions can be calculated by Equations 7-9:

$$D_c = \frac{\left\langle r_c^2(t) \right\rangle}{2t} \tag{7}$$

$$D_{ab} = \frac{\left\langle r_{ab}^2(t) \right\rangle}{4t} \tag{8}$$

$$D_{3D} = \frac{\left\langle r_{abc}^2(t) \right\rangle}{6t} \tag{9}$$

Each diffusion coefficient was calculated by fitting the MSD as a function of time (see Supplementary Material S_ for an example). All diffusion simuations were performed in NVT emsamble by extensive simulation time of 1 ns to ensure adequate statistical sampling. Migration energy barriers (E_m) for each ion travelling along potential diffusion paths were found by NEB analysis. [PENGHUI, PLEASE EXPLAIN THE NEB PROCESS HERE]. An example of how this process was applied to the simulations in this manuscript is shown in Supplementary Material S_. Finally, calculated diffusion coefficients were extrapolated to lower temperatures, by scaling the values found using Equations 7-9 by the difference in

All input files, intermediate files, raw output files, scripts, intermediate and final results can be found alongside this article and its supplementary material in our permanent GitHub repository for this paper [REF].

3 Results

3.1 Thermodynamics of Defect Formation

- Describe E_f for vacancies and interstitials in Cr_2O_3, so the $C(T)$ term in Equation 3 can be known.

3.2 Temperature-Dependent Ion Diffusivities

- Diffusion coefficients determined at vacancy defect interstital defect are shown in Fig. 2 and 3.
- Also show Ni and Fe effects on oxygen diffusion here

3.3 Ion Migration Pathways

- Oxygen vacancy migration pathways, Fig. 4
- Chromium vacancy migration pathways, Fig. 5
- Chromium interstitial migration pathway, Fig. 6
- Add a table of migration pathways
- Mention video files of oxygen and chromium migration in the Supplementary Material

4 Discussion

1. First, discuss the magnitudes & values of our calculated diffusion coefficients compared to literature (Lobnig, Sabioni) and simulations (Vaari). Explicitly say why they agree or don't.
   (a) VERY CLEARLY explain why Vaari's total 3D diffusion coefficients differ so much from ours in magnitude. Did he use a different potential? Different parameters? Why is it so different?
2. Explicitly state which direction (in-plane or out-of-plane) is slower, and by how much. This is the direction that we want to induce for slower corrosion rates. Compare this difference in diffusivity with the corrosion rate differences in [3, 2] for the most direct comparison.

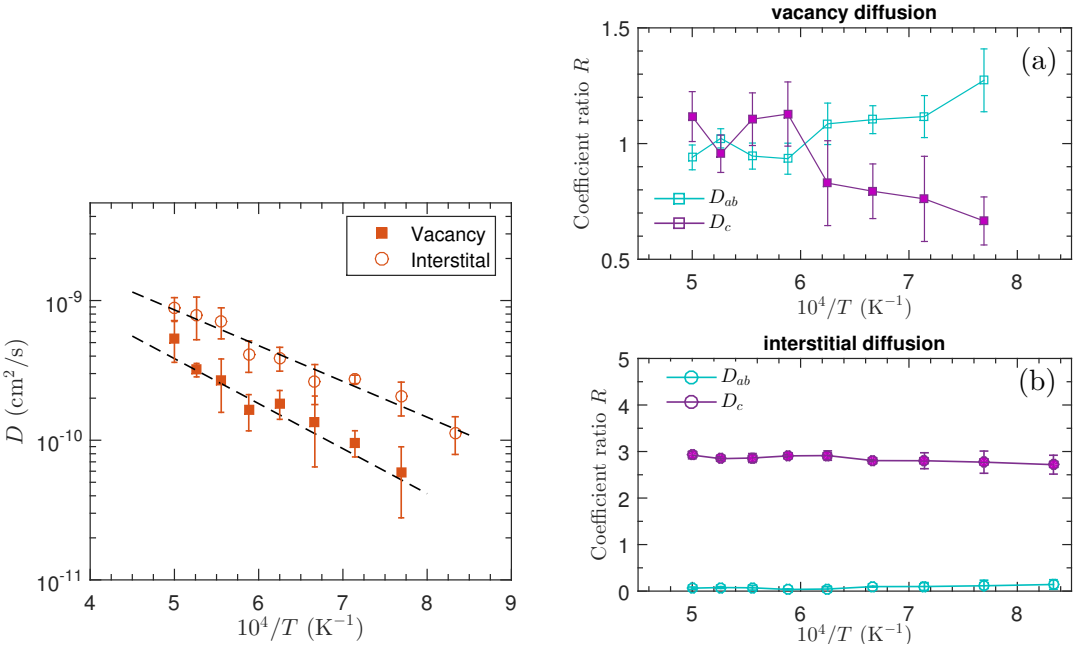

Figure 2: Chromium ion diffusivities in 3 dimensions, along c axis and in ab plane. (left)Oxygen vacancy and intersti- tial diffusion coefficients as function of temperature, (right) (a)normalized chromium vacancy diffusivities D ab and D c in ab plan and along c axis, (b)normalized chromium interstital diffusivities in ab plan and along c axis

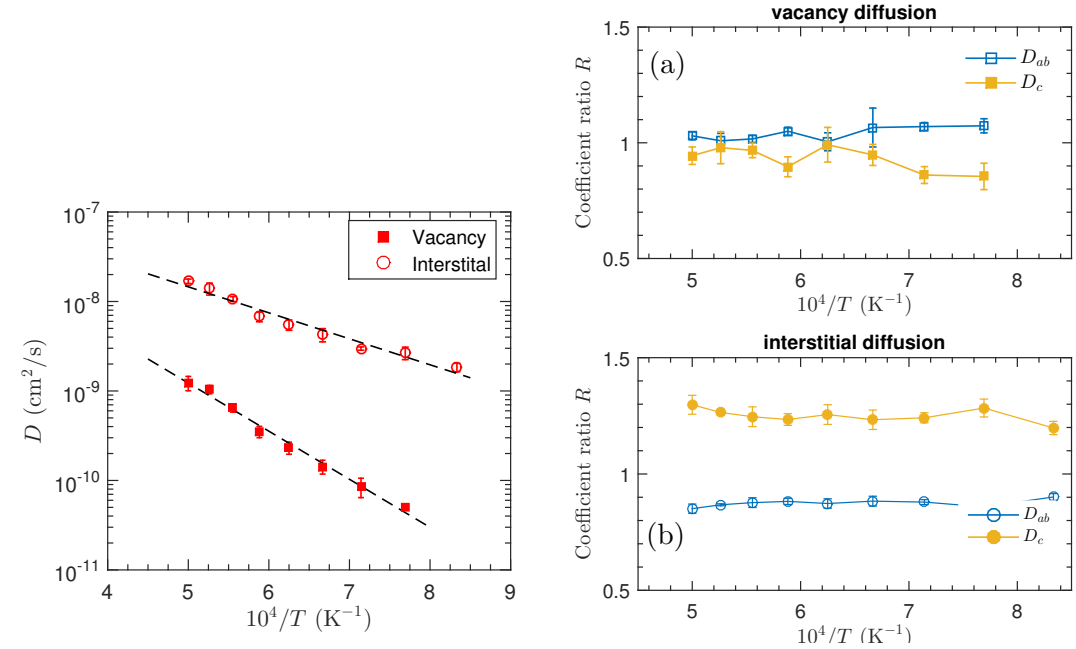

Figure 3: Oxygen ion diffusivities in 3 dimensions, along c axis and in ab plane. (left)oxygen vacancy and interstitial diffusion coefficients as function of temperature, (right) (a)normalized oxygen vacancy diffusivities D ab and D c in ab plan and along c axis, (b)normalized oxygen interstital diffusivities in ab plan and along c axis

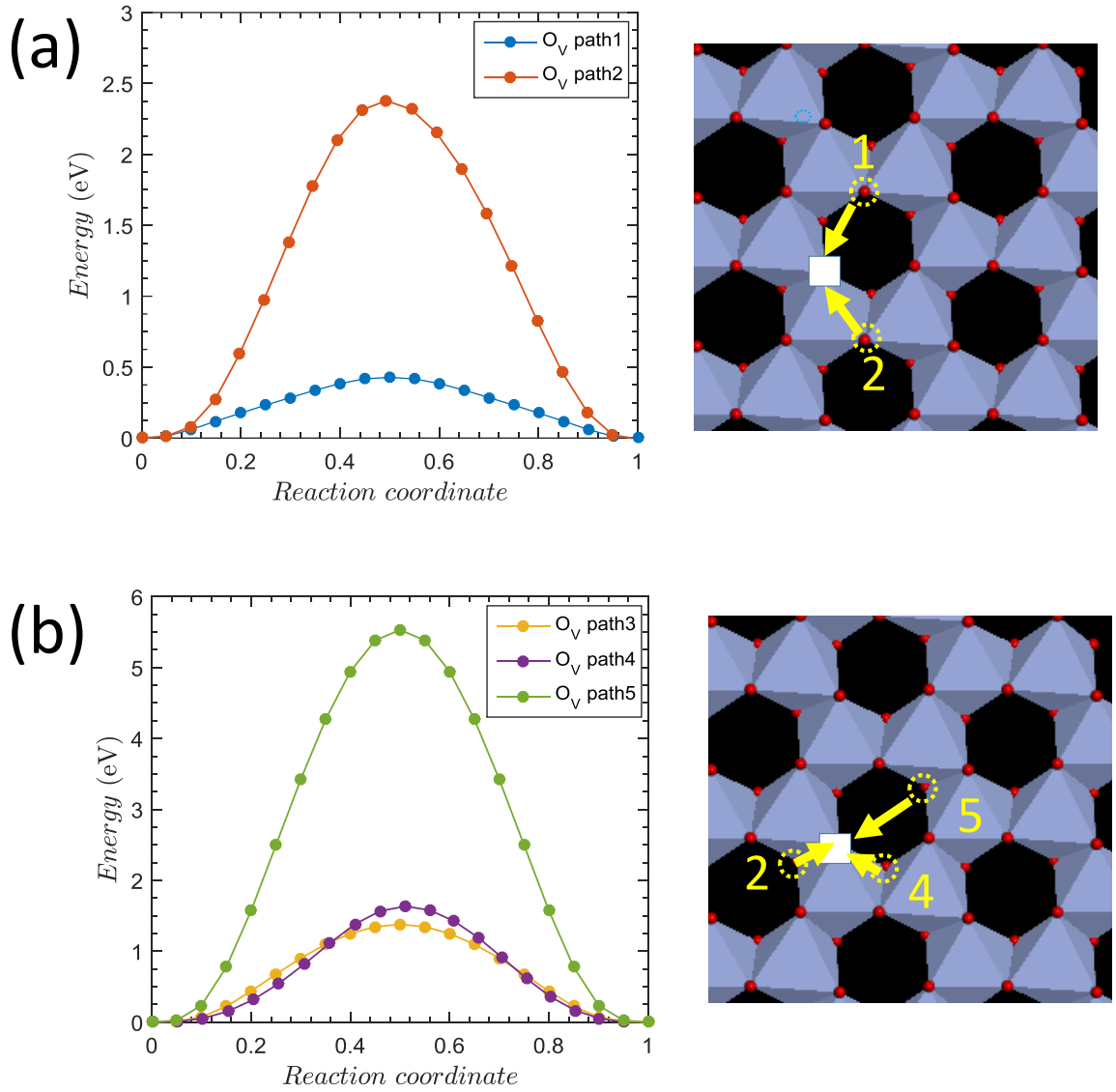

Figure 4: Oxygen vacancy migration pathways. (a) paths in ab plane, (b) out of plane paths

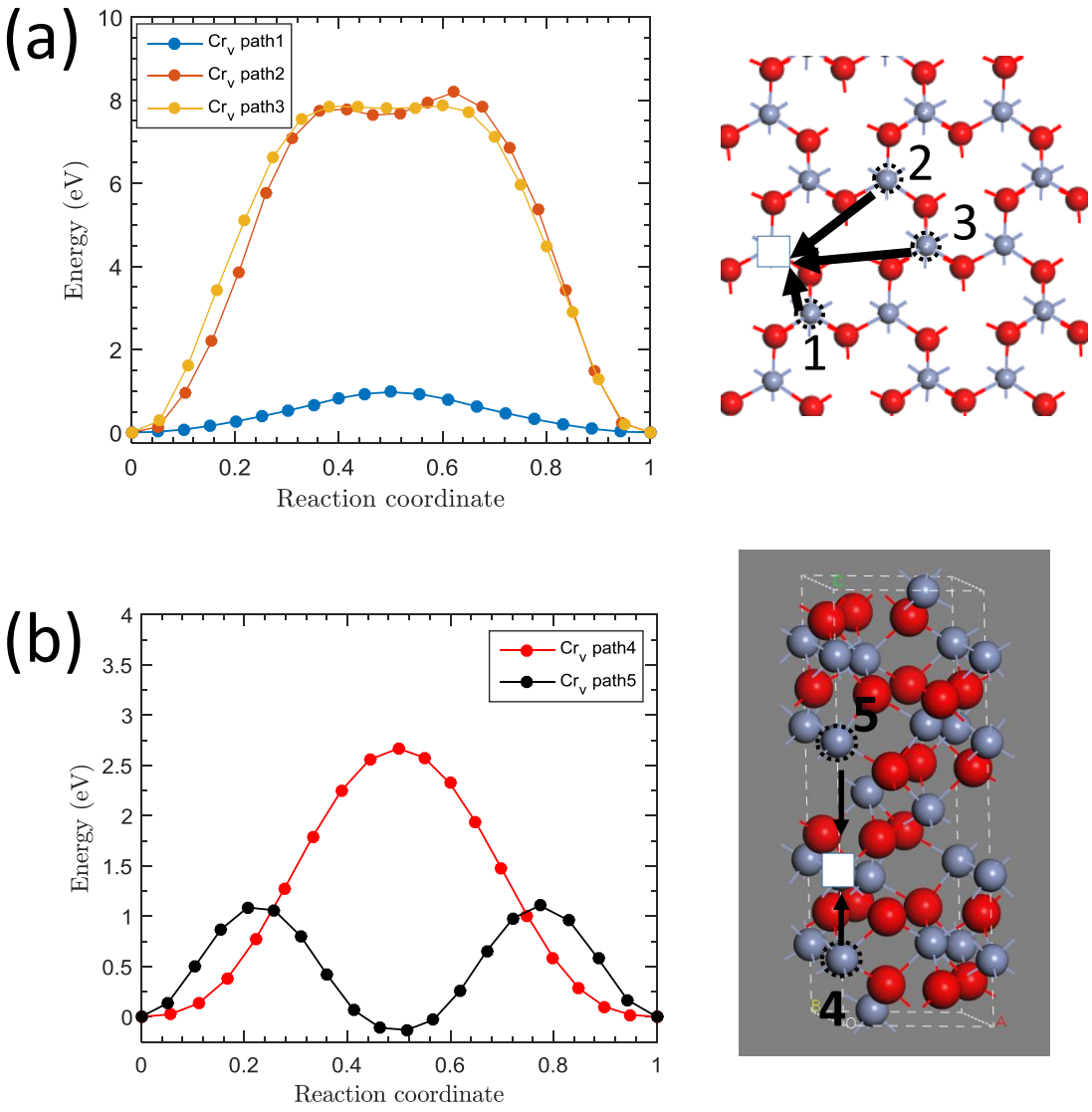

Figure 5: Chromium vacancy migration pathways. (a) paths in ab plane, (b) out of plane paths

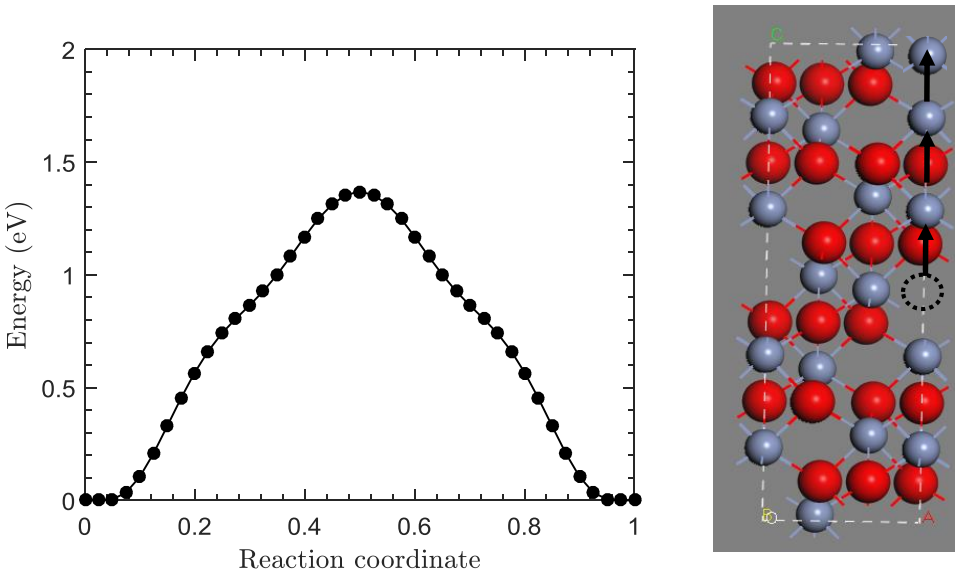

Figure 6: Chromium interstitial migration pathway

3. Mention how some studies show grain boundary diffusion to be 1,000x times faster than the effective diffusivity [14], though controversy still exists whether it's bulk or GB dominated transport [WE SHOULD FIND MORE LITERATURE DISCUSSING THIS]

4. Talk about what should be done to confirm whether this effect is real, and *utilizable*.

   (a) Need explicit measurements of Cr_2O_3 texture via EBSD as a function of processing (cast, annealed, rolled, forged, SPD)

   (b) Need explicit measurements of tracer diffusion rates in differently oriented single crystals of Cr_2O_3 to confirm our measurements

   (c) Need to try actual corrosion experiments on as-manufactured materials by different processes to confirm

5 Conclusions

(will write last)

Acknowledgements

P. C. and M. P. S. gratefully acknowledge support from the Electric Power Research Institute's (EPRI's) Pressurized Water Reactors Technical Advisory Committee (P-TAC), under contract number ___.

References

[1] International Stainless Steel Forum (ISSF). Stainless steel in figures: 2015. Technical report, International Stainless Steel Forum (ISSF), 2015.

[2] B. Ravi Kumar, Raghuvir Singh, Bhupeshwar Mahato, P.K. De, N.R. Bandyopadhyay, and D.K. Bhattacharya. Effect of texture on corrosion behavior of aisi 304l stainless steel. *Mater. Charact.*, 54(2):141–147, February 2005.

[3] Arash Shahryari, Jerzy A. Szpunar, and Sasha Omanovic. The influence of crystallographic orientation distribution on 316lvm stainless steel pitting behavior. *Corros. Sci.*, 51(3):677–682, March 2009.

[4] S. Kudelka, A. Michaelis, and J.W. Schultze. Electrochemical characterisation of oxide layers on single grains of a polycrystalline ti-sample. *Berichte der Bunsengesellschaft fÃŒr physikalische Chemie*, 99(8):1020–1027, 1995.

[5] Majid Hoseini, Arash Shahryari, Sasha Omanovic, and Jerzy A. Szpunar. Comparative effect of grain size and texture on the corrosion behaviour of commercially pure titanium processed by equal channel angular pressing. *Corros. Sci.*, 51(12):3064–3067, December 2009.

[6] Brian E. Conway and Gregory Jerkiewicz. Surface orientation dependence of oxide film growth at platinum single crystals. *J. Electroanal. Chem.*, 339(1-2):123–146, November 1992.

[7] D. A. Jones. *Principles and prevention of corrosion, 2nd ed.* Prentice Hall, 1996. ISBN-13: 978-0133599930.

[8] Alexander Chroneos, David Parfitt, John A. Kilner, and Robin W. Grimes. Anisotropic oxygen diffusion in tetragonal la2nio4+[small delta]: molecular dynamics calculations. *J. Mater. Chem.*, 20:266–270, 2010.

[9] Emma Kendrick, John Kendrick, Kevin S. Knight, M. Saiful Islam, and Peter R. Slater. Cooperative mechanisms of fast-ion conduction in gallium-based oxides with tetrahedral moieties. *Nat Mater*, 6(11):871–875, November 2007.

[10] Alexander Chroneos, Bilge Yildiz, Albert Tarancon, David Parfitt, and John A. Kilner. Oxygen diffusion in solid oxide fuel cell cathode and electrolyte materials: mechanistic insights from atomistic simulations. *Energy Environ. Sci.*, 4:2774–2789, 2011.

[11] David Parfitt, Alexander Chroneos, Albert Tarancon, and John A. Kilner. Oxygen ion diffusion in cation ordered/disordered gdbaco2o5+d. *J. Mater. Chem.*, 21:2183–2186, 2011.

[12] William C. Hagel. Anion diffusion in a-cr2o3. *J. Am. Ceram. Soc.*, 48(2):70–75, 1965.

[13] A. C. S. Sabioni, A. M. Huntz, F. Millot, and C. Monty. Self-diffusion in cr2o3 ii. oxygen diffusion in single crystals. *Philosophical Magazine A*, 66(3):351–360, September 1992.

[14] A.C.S. Sabioni, A.M. Huntz, F. Silva, and F. Jomard. Diffusion of iron in cr2o3: polycrystals and thin films. *Materials Science and Engineering: A*, 392(1-2):254–261, February 2005.

[15] Antônio Claret Soares Sabioni, Roberto Paulo Barbosa Ramos, Vincent Ji, François Jomard, Waldemar Augusto de Almeida Macedo, Pedro Lana Gastelois, and Vicente Braz Trindade. About the role of chromium and oxygen ion diffusion on the growth mechanism of oxidation films of the aisi 304 austenitic stainless steel. *Oxid. Met.*, 78(3-4):211–220, 2012.

[16] A. C. S. Sabioni, A. M. Huntz, L. C. Borges, and F. Jomard. First study of manganese diffusion in cr2o3 polycrystals and thin films by sims. *Philos. Mag.*, 87(12):1921–1937, April 2007.

[17] RE Lobnig, HP Schmidt, K Hennesen, and HJ Grabke. Diffusion of cations in chromia layers grown on iron-base alloys. *Oxid. Met.*, 37(1-2):81–93, 1992.

[18] SC Tsai, AM Huntz, and C Dolin. Growth mechanism of cr2o3 scales: oxygen and chromium diffusion, oxidation kinetics and effect of yttrium. *Materials Science and Engineering: A*, 212(1):6–13, 1996.

[19] Kazutomo Hoshino and NL Peterson. Cation self-diffusion in cr2o3. *J. Am. Ceram. Soc.*, 66(11):c202–c203, 1983.

[20] C RICHARD A Catlow, JOHN CORISH, JOHN HENNESSY, and WILLIAM C MACKRODT. Atomistic simulation of defect structures and ion transport in α-fe2o3 and α-cr2o3. *J. Am. Ceram. Soc.*, 71(1):42–49, 1988.

[21] Jukka Vaari. Molecular dynamics simulations of vacancy diffusion in chromium(iii) oxide, hematite, magnetite and chromite. *Solid State Ionics*, 270:10–17, February 2015.

[22] Larry W. Finger and Robert M. Hazen. Crystal structure and isothermal compression of fe2o3, cr2o3, and v2o3 to 50 kbars. *J. Appl. Phys.*, 51(10):5362–5367, 1980.

[23] Steve Plimpton. Fast parallel algorithms for short-range molecular dynamics. *J. Comput. Phys.*, 117(1):1–19, March 1995.

[24] Robin W. Grimes, D. Jason Binks, and A. B. Lidiard. The extent of zinc oxide solution in zinc chromate spinel. *Philosophical Magazine A*, 72(3):651–668, September 1995.

[25] Licia Minervini, Robin W. Grimes, John A. Kilner, and Kurt E. Sickafus. Oxygen migration in lanio. *J. Mater. Chem.*, 10:2349–2354, 2000.